

All-dielectric photonic-assisted radio front-end technology

RICK C. J. HSU, ALI AYAZI, BIJAN HOUSHMAND AND BAHRAM JALALI*

Department of Electrical Engineering, University of California, Los Angeles, California 90095-1594, USA

*e-mail: jalali@ucla.edu

Published online: 19 August 2007; doi:10.1038/nphoton.2007.145

The threats to civil society posed by high-power electromagnetic weapons are viewed as a grim but real possibility in the world after 11 September 2001 (refs 1–3). These weapons produce a power surge capable of destroying or damaging sensitive circuitry in electronic systems. Unfortunately, the trend towards circuits with smaller sizes and voltages renders modern electronics highly susceptible to such damage. Radiofrequency communication systems are particularly vulnerable, because the antenna provides a direct port of entry for electromagnetic radiation. Here, we report a type of radiofrequency receiver front end featuring a complete absence of electronic circuitry and metal interconnects, the traditional ‘soft spots’ of a conventional radiofrequency receiver. The device exploits a dielectric resonator antenna to capture and deliver the radiofrequency signal onto an electro–optic field sensor. The dielectric approach has an added benefit in that it reduces the physical size of the front end, an important benefit in mobile applications.

The Graham Commission report, presented to the U.S. Congress’ House Committee on Armed Services on 22 July 2004, concluded that a ‘high-altitude nuclear electromagnetic pulse (HEMP) is one of the few threats that can hold at risk the continued existence of civil society in the United States. . . The current vulnerability of our critical infrastructures can both invite and reward attack if not corrected’³. Such HEMP and other types of high-power microwave (HPM) weapons can shut down telecommunications networks without leaving any trace of the attacker². They generate bursts of electromagnetic energy strong enough to damage or destroy electronic circuitry. Ironically, the danger is exacerbated by the impact of the celebrated Moore’s law, which describes the electronic industry’s relentless pursuit of miniaturization. The scaling has resulted in a continued reduction in the maximum voltage that such circuits can tolerate, rendering modern electronics highly susceptible to damage from high-power electromagnetic sources. For example, voltages as low as 10 V can punch through the gate oxide of a modern CMOS transistor. This value should be compared with the capabilities of HPM weapons, which can deliver transient potentials of tens of kilovolts inside a circuit. Catastrophic damage also results from melting and arcing of metallic interconnects by the large current surge produced by the HPM source². Even less intense bursts can permanently damage circuits, causing them to fail at a later time².

Although most components in a system can be protected using Faraday cages, the front-end components in a communication system are particularly vulnerable, because the antenna provides

a direct path for an electromagnetic pulse to enter the system. The conventional method for protecting circuits against high transient voltages uses a shunt diode to limit the voltage, but this method is best suited for lower frequencies⁴. At high frequencies (>5 GHz), the addition of the diode capacitance to the input node of the low-noise amplifier will compromise the bandwidth and noise performance of the receiver. Although steady incremental progress is being made in applying this technique to high-frequency circuits, the fundamental and intrinsic limitation owing to loading of the amplifier’s input node remains. Because of the weak signal levels and sensitive electronics (the low-noise amplifier), the receiver is more vulnerable and more difficult to protect than the transmitter in a radiofrequency (RF) front end. Presently, there are few options for protecting high-frequency receivers from high-power electromagnetic radiation. The proposed all-dielectric photonic-assisted radio front-end technology is aimed at addressing this need.

The vulnerability to HPMs can be mitigated by eliminating all metallic components and transistors in the RF front end, and by providing charge isolation between the front end and downstream electronic data-processing circuitry. We create such a device by combining a dielectric antenna with an electro–optic crystal field sensor. Figure 1 shows a conceptual description of this all-dielectric photonic-assisted radio front-end technology. The dielectric antenna is a leaky resonator that is fabricated from a material with low loss and high relative permittivity. The incoming signal, in the form of a free-space electromagnetic field, excites a resonance mode of the antenna resulting in a desired buildup of field inside the structure. We exploit this enhanced electric field to modulate an optical carrier in a linear electro–optic crystal. To enhance the receiver sensitivity, the crystal is formed into a resonator. Such resonators have previously been used to create electro–optic modulators based on metal electrodes and demonstrating simultaneous optical and RF resonances^{5–10}. An optical waveguide, such as a single-mode fibre, transfers the signal to the system back end, where a photodetector converts it to an electrical signal that is subsequently processed using conventional electronics.

The novelty behind this technology is multifold. First, the antenna itself is made of only dielectric materials. With no metallic electrodes and interconnects present in the front end, the high-field damage caused by arcing or melting of metallic components is eliminated. Second, the subsequent electrical–optical–electrical conversion provides charge isolation. Our device exploits this function in a similar manner to an optocoupler—a common

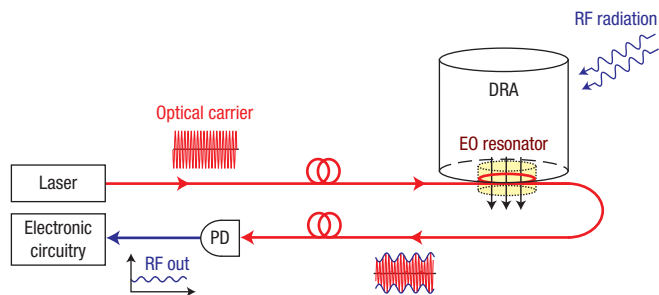


Figure 1 Concept of the photonic-assisted all-dielectric RF front-end technology. An electro–optic (EO) powered dielectric antenna captures the free-space RF signal. The embedded optical link provides complete electrical isolation between the air interface and the electronic circuitry, which is located only after the photodetector (PD).

device that creates electrical isolation between two nodes of a low-speed digital circuit (by using an LED and a photodetector to create a short optical link between them). However, there are critical differences between the optocoupler and the technology we present here. The traditional optocoupler uses semiconductor devices, metallic interconnects, and electrodes. Furthermore, its use is limited to situations where standard digital logic signals are used. The device lacks the high-frequency response and the sensitivity that is required in an analogue RF receiver. The third advantage of the proposed device derives from the fact that the dielectric antenna is made of high-permittivity materials and is smaller than conventional metallic antennas, resulting in a highly compact front end. In fact, antenna size reduction is the main motivation for use of dielectric antennas in conventional applications^{11–14}. Yet another advantage is the higher quality factor (Q) of the dielectric antenna compared with a metallic antenna, in particular at high frequencies.

We chose a cylindrical geometry for the dielectric resonant antenna (DRA) and performed the design using finite-element simulations carried out with the High-Frequency Structure Simulator (HFSS, Ansoft Corporation). The optimum location for the electro–optic crystal is the position inside the DRA where the maximum RF field enhancement occurs. One of the objectives of finite-element simulations is to identify this location, which in turn depends on the resonant mode of the DRA. The design reported here takes advantage of the $TM_{011+\delta}$ mode of the DRA, because it provides a high electric field on the top and bottom cylinder surfaces, with field lines that are perpendicular to these surfaces. The electro–optic crystal can then be placed outside the cylinder, as shown in Fig. 2a. Although this geometry is not the optimum in terms of receiver sensitivity, it eliminates the need to embed the crystal inside the DRA. This simplifies device packaging, facilitates the proof-of-concept demonstration, and is the main motivation for our choice of the cylindrical DRA design. Details of the DRA antenna and the $LiNbO_3$ disk resonator are described in the Methods section.

Figure 3 indicates the typical RF sensitivities that our receiver technology can achieve. The model used for these calculations is described in the Methods section. As an example, an RF sensitivity of -150 dBm Hz⁻¹ can be achieved using a common distributed-feedback (DFB) laser that produces an average power of 10 mW and has a relative intensity noise (RIN) of -150 dB. This is approximately 10 dB better than the requirements of a WiFi receiver (IEEE 802.11 a). The performance can be further improved with DRA optimization.

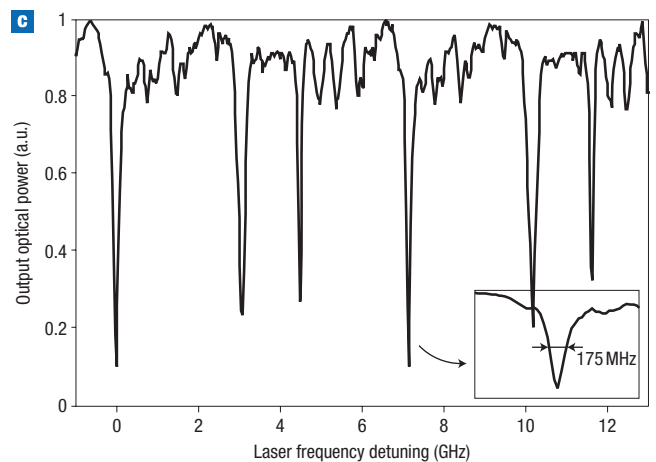
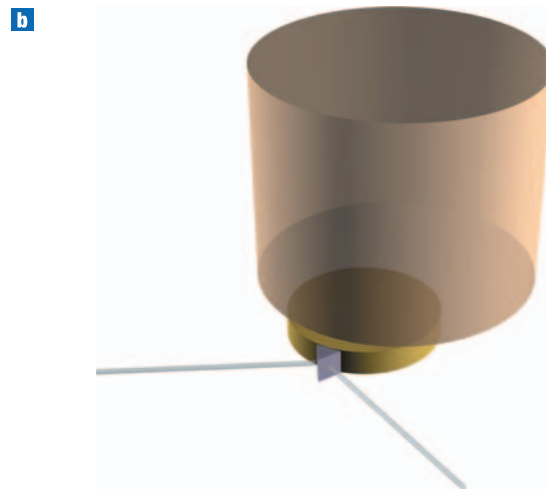
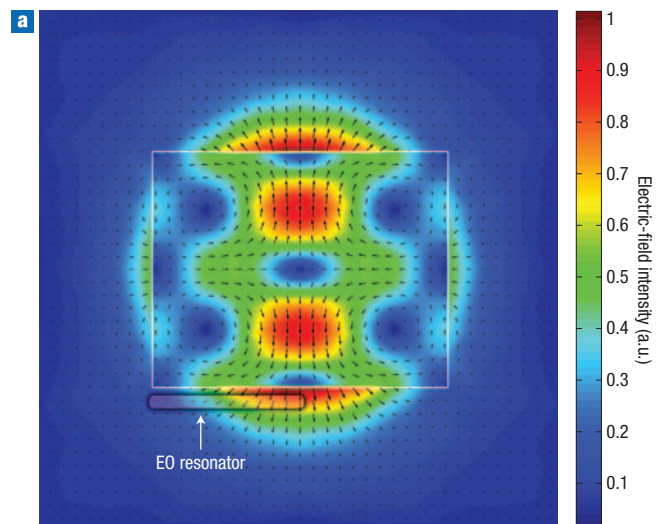


Figure 2 Details of the receiver front-end design and the resonance spectrum of the electro–optic (EO) resonator. **a**, Numerical simulation of the distribution of the electric field of the $TM_{011+\delta}$ mode inside a cylindrical DRA (11.25 mm in diameter, 9 mm high). **b**, Three-dimensional drawing of the DRA integrated with an electro–optic microdisk resonator. **c**, The optical resonance spectrum of the TE whispering-gallery modes in the $LiNbO_3$ microdisk resonator; diameter = 5.9 mm, FSR = 7.38 GHz, $Q \sim 1.1 \times 10^6$.

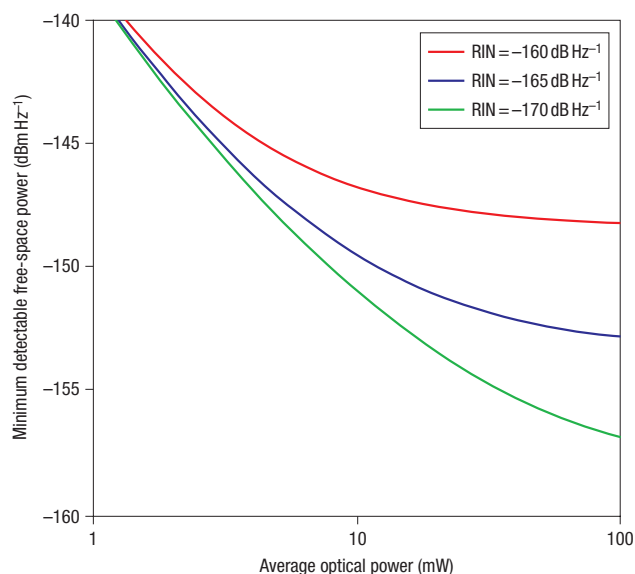


Figure 3 Receiver sensitivity. Calculated receiver sensitivity versus average optical power incident on the photodetector. A constant laser RIN noise was assumed. The sensitivity is a strong function of laser power and RIN level. The model used for sensitivity calculation is described in the Methods section and the following parameters are used in the calculation: optical FSR (receiver centre frequency) = 10 GHz, $\beta = 25$, $\epsilon_{\text{DRA}} = 38$, $\epsilon_{\text{LN}} = 35$, $F = 100$, $R = 0.8$, $r_{33} = 30.8 \text{ pm V}^{-1}$, $A_e = 10^{-4} \text{ m}^2$, $n_e = 2.14$, and $\lambda = 1.55 \text{ }\mu\text{m}$.

To demonstrate the device experimentally, we used a set-up similar to that shown in Fig. 1. Light from a tunable laser was coupled to a microdisk resonator using a diamond prism. A horn antenna illuminated the receiver with a 7.38 GHz RF signal. A photodetector module (Discovery DSC40S) followed by an RF amplifier (Picosecond Lab 5840B) performed opto–electronic conversion. The received signal was analysed on an RF spectrum analyser. The detector had a responsivity of 0.8 A W^{-1} , which translates to 40 V W^{-1} conversion gain on a load of $50 \text{ }\Omega$. In our experiments, the optical power incident on the photodetector was 6 mW. The overall receiver had a bandwidth (-3 dB) of 35 MHz, determined primarily by the RF resonance within the DRA.

Figure 4 shows the received signal power on the spectrum analyser with and without the dielectric antenna. As the DRA is removed from the LiNbO_3 crystal, the signal level decreases by 40 dB. The RF spectrum analyser's resolution bandwidth was set to 10 kHz. The observed noise floor of -136 dBm Hz^{-1} (-96 dBm over 10 kHz instrument bandwidth) is generated by the RIN of the source laser. Figure 5 shows the received RF power versus the free-space power impinging on the dielectric antenna cross-section. The free-space power was obtained by calculating the fraction of the power fed into the horn antenna falling onto the dielectric antenna using a standard model for the radiation pattern of the horn antenna¹⁵. The minimum detectable free-space RF power is -57 dBm or equivalently -97 dBm Hz^{-1} . This corresponds to a minimum detectable electric field of $8.7 \times 10^{-4} \text{ V m Hz}^{-1/2}$ and is limited by the laser RIN noise. The maximum RF power applied to the horn antenna was limited to 20 dBm by the available RF source.

The demodulated signal power is 37 dB weaker than the total RF power impinging on the DRA cross-section. Achieving better RF-to-optical-to-RF conversion gain will require more optical power. Furthermore, for ease of integration, the LiNbO_3

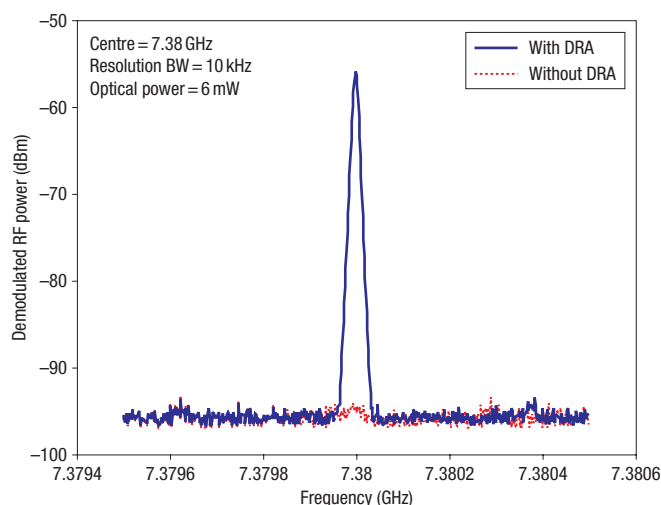


Figure 4 Detection of the free-space RF signal by the prototype receiver.

The response of the all-dielectric photonic-assisted RF receiver to the 7.38 GHz EM wave transmitted by the horn antenna with (blue solid line) and without (red dashed line) the DRA in the front end. The resolution bandwidth (BW) of the RF spectrum analyser is set to 10 kHz.

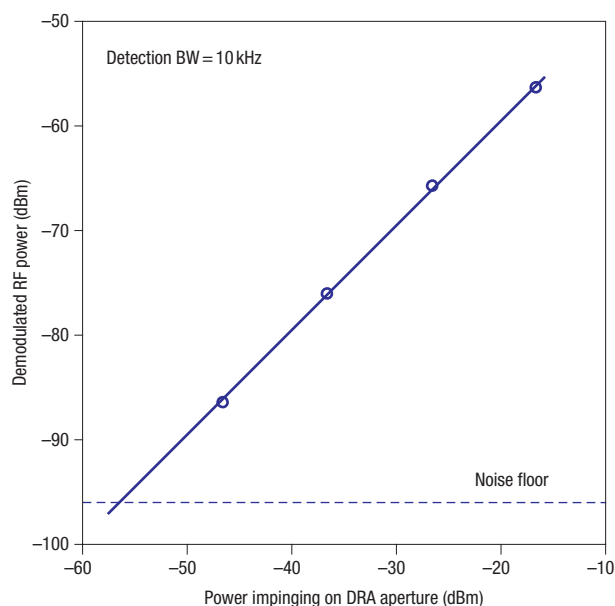


Figure 5 Measured sensitivity of the prototype receiver. Plotting the demodulated RF power (after photodetection) versus the total power impinging on the DRA aperture shows the response of the all-dielectric photonic-assisted RF receiver. The measured minimum detectable free-space power is -97 dBm Hz^{-1} and the noise floor is limited by laser RIN.

resonator was placed outside the DRA. For optimum performance the LiNbO_3 resonator can be integrated within the DRA where the maximum electric field resides.

A comment about the high field immunity of the proposed device is called for. The dielectric strengths of DRA and LiNbO_3 materials are about 10^5 V cm^{-1} (refs 16, 17), similar to those in common semiconductors and dielectrics used in

integrated-circuit manufacturing. However, in a typical integrated circuit, voltage surge appears across the gate insulator of the front-end transistor, which is in the order of 100 nm or less in a high-speed transistor. In the dielectric antenna, this dimension is in the order of the free-space RF wavelength divided by the square root of the dielectric constant, resulting in a value of approximately 6 mm (10 GHz signal and a dielectric constant of 36). Even with a field enhancement factor of 20 (18 in the prototype device), the electric field inside the DRA (and the LiNbO₃) will be a factor of 10³–10⁴ lower than that occurring in the front-end transistor.

In summary, we have reported a new type of RF receiver featuring absolutely no metal electrodes, interconnects and transistors in the front end. By eliminating the soft spots of a conventional receiver, the new technology is aimed at addressing the vulnerability of today's wireless communication and radar systems.

METHODS

DIELECTRIC ANTENNA

The DRA material used was a composite ceramic (BaTiO₃-based) with relative permittivity $\epsilon_r = 38$ and a loss tangent of 0.0005 at microwave frequencies. The dimensions are fine-tuned (11.25 mm in diameter, 9 mm high) to give TM_{011+ δ} resonance at 7.38 GHz, to match the free spectral range (FSR) of the optical resonator (the reason for this will be explained later). Figure 2a shows the electric-field pattern when the DRA is excited by a 7.38 GHz plane wave incident from the broad side. The field-enhancement factor (β), defined as the ratio of DRA-enhanced field strength to the incident free-space field, is approximately 18 at the location just below the DRA bottom surface and along the centre axis. This quantity affects the receiver sensitivity as described below. The far-field pattern of the TM_{011+ δ} mode in a cylindrical DRA is known to resemble that of an electric quadrupole¹⁴.

ELECTRO–OPTIC RESONATOR

The electro–optic disk resonator is made of a Z-cut LiNbO₃. These structures exhibit high-Q whispering-gallery resonant modes and their fabrication and performance characteristics have been described elsewhere^{5–9}. The resonator used here has a radius $r = 2.85$ mm, an FSR = 7.38 GHz and a loaded quality factor of $Q \sim 1.1 \times 10^6$, corresponding to a finesse of $F \sim 42$, and a bandwidth of 175 MHz at 1.55 μm , as shown in Fig. 2c. Because of the long photon lifetime in the high-Q resonator, photons interact with the electric field on multiple passes, resulting in improved sensitivity to the RF field (E_{RF}). When a TE polarized optical field is interacting with a modulating electric field, $E_{\text{RF}} = E_m \sin(2\pi f_m t)$, where E_m is the amplitude of the modulating field and f_m is the modulation frequency, of the same orientation (along the c-axis of LiNbO₃), the round-trip phase shift θ can be written as

$$\theta = \frac{2\pi n_e L}{\lambda} + \delta \sin(2\pi f_m t - \varphi), \quad \varphi = \pi f_m n_e L_{\text{eff}} / c$$

$$\delta = \frac{\pi n_e^3 r_{33} E_m L_{\text{eff}}}{\lambda} \text{sinc}\left(\frac{\pi f_m n_e L_{\text{eff}}}{c}\right) = \frac{\pi E_m L_{\text{eff}}}{2 E_\pi L} \text{sinc}\left(\frac{\pi f_m n_e L_{\text{eff}}}{c}\right) \quad (1)$$

where $L = 2\pi r$ is the circumference of the disk, n_e is the extraordinary index of refraction at the operation wavelength λ , c is the speed of light in a vacuum and L_{eff} accounts for the effective modulation length where the modulating electric field and the optical wave overlap. The half-wave field E_π is defined as $E_\pi = \lambda / (2n_e^3 r_{33} L)$, where λ is the optical wavelength and r_{33} is the electro–optic coefficient. When the input laser frequency (f_0) is tuned to a particular optical resonance mode, high-frequency modulation can be achieved if the modulation sidebands reside in adjacent optical resonance modes, that is, when f_m is equal to the optical FSR. If the electro–optic resonator is critically coupled, the maximum slope point occurs when the laser is tuned to about 25% of the electric peak transmission. However, the modulating electric field (E_{RF}) applied to the

resonator may not be uniform across the disk, because as $L_{\text{eff}} = L$, δ goes to zero, and no sideband will be generated at $f_0 \pm f_m$. Optimal modulation efficiency occurs when $L_{\text{eff}} = L/2$. To approximate this condition, the electro–optic resonator is placed off-centre from the symmetrical axis of the DRA (Fig. 2b). In the optimal case ($L_{\text{eff}} = L/2$), the intensity modulation index is $m = 9F\delta/2(\sqrt{3})\pi$ and the system carrier-to-noise ratio $\text{CNR} = (mRP_0)^2/2\sigma_T^2$, where R is the photodetector responsivity, P_0 is the average optical power and σ_T^2 is the total variance of noise current, consisting of contributions from thermal noise, shot noise and the laser RIN.

RECEIVER SENSITIVITY

An analytical expression for the sensitivity of our receiver is obtained by finding the free-space RF power that results in a unity CNR at the photodetector. The result is given by

$$P_{\text{m,min}} = \left(\frac{E_{\text{m,min}} \epsilon_{\text{LN}}}{\beta \epsilon_{\text{DRA}}}\right)^2 \frac{A_c}{\eta} \quad (2)$$

where A_c is the DRA cross-section, η is the impedance of free space (377 Ω) and ϵ_{DRA} and ϵ_{LN} are the dielectric constants of the DRA and LiNbO₃ at microwave frequencies, respectively. $E_{\text{m,min}}$ is the minimum electric field that must be applied across LiNbO₃ to achieve a CNR of unity and is given by

$$E_{\text{m,min}} = \frac{4\pi E_\pi}{9RP_0 F} \sqrt{6\sigma_T^2} \quad (3)$$

Received 16 January 2007; accepted 25 June 2007; published 19 August 2007.

References

- Special Issue on High-Power Electromagnetics (HPEM) and Intentional Electromagnetic Interference (IEMI). *IEEE Trans. EMC* **46**, 314–321 (2004).
- Abrams, M. Dawn of the e-bomb. *IEEE Spectrum* **40**, 24–30 (2003).
- U.S. Congress. Report of the Commission to Assess the Threat to the United States from Electromagnetic Pulse (EMP) Attack, Vol. 1, Executive Report (2004), http://www.globalsecurity.org/wmd/library/congress/2004_r/04-07-22emp.pdf
- Gong, K., Feng, H., Zhan, R. & Wang, A. Z. H. A study of parasitic effects of ESD protection on RF ICs. *IEEE Trans. Microwave Theory Technol.* **50**, 393–402 (2002).
- Ilchenko, V. S., Savchenkov, A. A., Matsko, A. B. & Maleki, L. Sub-microwatt photonic microwave receiver. *IEEE Photon. Technol. Lett.* **14**, 1602–1604 (2002).
- Ilchenko, V. S., Savchenkov, A. A., Matsko, A. B. & Maleki, L. Whispering-gallery-mode electro-optic modulator and photonic microwave receiver. *J. Opt. Soc. Am. B* **20**, 333–341 (2003).
- Cohen, D. A., Houssein-Zadeh, M. & Levi, A. F. J. Microphotonic modulator for a microwave receiver. *IEEE Electron. Lett.* **37**, 300–301 (2001).
- Cohen, D. A. & Levi, A. F. J. Microphotonic components for a mm-wave receiver. *Solid State Electron.* **45**, 495–505 (2001).
- Houssein-Zadeh, M. & Levi, A. F. J. 14.6-GHz LiNbO₃ microdisk photonic self-homodyne RF receiver. *IEEE Trans. Microwave Theory Tech.* **54**, 821–831 (2006).
- Tazawa, H. *et al.* Ring resonator-based electrooptic polymer traveling-wave modulator. *IEEE J. Lightwave Technol.* **24**, 3514–3519 (2006).
- Dettmer, R. Dielectric antenna make waves. *IEEE Rev.* **49**, 28–31 (2003).
- Petosa, A., Ittipiboon, A., Antar, Y. M. M., Roscoe, D. & Cuhaci, M. Recent advances in dielectric resonator antenna technology. *IEEE Trans. Antennas Propag.* **40**, 35–48 (1998).
- Long, S. A., McAllister, M. & Shen, L. C. The resonant cylindrical dielectric cavity antenna. *IEEE Trans. Antennas Propag.* **31**, 406–412 (1983).
- Mongia, R. K. & Bhartia, P. Dielectric resonator antennas – a review and general design relations for resonant frequency and bandwidth. *Int. J. Microwave Millimeter-Wave Computer-Aided Engineering* **4**, 230–247 (1991).
- Institute of Electrical and Electronic Engineers, *IEEE standard methods for measuring electromagnetic field strength of sinusoidal continuous waves, 30 Hz to 30 GHz* no. IEEE Std 291-1991, (IEEE, New York, 1991).
- Panteny, S., Stevens, R. & Bowen, C. R. Characterisation and modelling of barium titanate–silver composites. *Integr. Ferroelectr.* **63**, 131–135 (2004).
- Tamir, T. *Guided-Wave Optoelectronics* (Spring-Verlag, Berlin, Heidelberg, 1988).

Acknowledgements

This work was supported by DARPA and the U.S. Army. We are grateful to L. Maleki of the Jet Propulsion Laboratory for providing the LiNbO₃ microdisk resonator, and to W. Steier of USC, Tatsuo Itoh and D. Solli of UCLA for helpful discussions. Correspondence and requests for materials should be addressed to B.J.

Competing financial interests

The authors declare no competing financial interests.

Reprints and permission information is available online at <http://npg.nature.com/reprintsandpermissions/>